CHAPTER ONE

Super-Accuracy and Super-Resolution: Getting Around the Diffraction Limit

Erdal Toprak,[*,†] Comert Kural,[*,‡] *and* Paul R. Selvin[*,§]

Contents

Abstract

In many research areas such as biology, biochemistry, and biophysics, measuring distances or identifying and counting objects can be of great importance. To do this, researchers often need complicated and expensive tools in order to have accurate measurements. In addition, these measurements are often done under nonphysiological settings. X-ray diffraction, for example, gets Angstrom-level structures, but it requires crystallizing a biological specimen. Electron microscopy (EM) has about 10 Å resolution, but often requires frozen (liquid nitrogen) samples. Optical microscopy, while coming closest to physiologically relevant conditions, has been limited by the minimum distances to be measured, typically about the diffraction limit, or ~200 nm. However, most

* Department of Biophysics, University of Illinois, Urbana, Illinois, USA
† Department of Systems Biology, Harvard Medical School, Boston, Massachusetts, USA
‡ Immune Disease Institute, Harvard Medical School, Boston, Massachusetts, USA
§ Department of Physics, University of Illinois, Urbana, Illinois, USA

Methods in Enzymology, Volume 475
ISSN 0076-6879, DOI: 10.1016/S0076-6879(10)75001-1
© 2010 Elsevier Inc.
All rights reserved.

biological molecules are <5–10 nm in diameter, and getting molecular details requires imaging at this scale. In this chapter, we will describe some of the experimental approaches, from our lab and others, that push the limits of localization accuracy and optical resolution in fluorescence microscopy.

1. Overview: Accuracy and Resolution

There are actually two fundamentally different types of limits, namely, *accuracy* and *resolution*. In general, the historic limit on how well you can do has been the Rayleigh diffraction limit of light, or about 200 nm. Modern techniques reach up to approximately a nanometer or two in accuracy, and 20 nm in the minimum distance between identical points, which is resolution.

Accuracy is the minimum distance or volume that one can locate a particle's position within a certain time period. Our lab has generally focused on enhancing the localization accuracy of single-molecule microscopy, often called super-accuracy. Our work on fluorescence imaging with one nanometer accuracy (FIONA) achieves $\sim$1 nm accuracy in 1–500 ms. FIONA has been applied to *in vitro* and *in vivo* samples, and to living organisms (Kural *et al.*, 2005, 2009; Yildiz *et al.*, 2003). It can be extended to nonfluorescent (absorbing) probes as well (Kural *et al.*, 2007). Naturally, FIONA is just the culmination of a long string of work in an effort to reach super-accuracy (Bobroff, 1986; Gelles *et al.*, 1988; Ghosh and Webb, 1994; Schmidt *et al.*, 1996).

Resolution is the minimum distance or volume that can be measured *between* two (identical) particles in a given period of time. For visible fluorescence in the far-field, it is $\sim\lambda/2$ or $\sim$200–300 nm. However, with modern super-resolution methods, the optical resolution is brought down to $\sim$8–25 nm. The general idea is to have two fluorophores where they can be separately imaged, because they either emit or are excited at different wavelengths, or can be temporarily or permanently turned off. As long as there is only a single emitting fluorophore left at one time within a diffraction-limited spot, it can be localized to high precision via a FIONA type of measurement. The process is then repeated many times, and the full high-resolution image is reconstructed (more on super-accuracy and super-resolution later).

Most super-accuracy and super-resolution techniques rely on imaging single molecules. The technology for single-molecule biophysics was pioneered in the late 1970s by a handful of researchers. In 1976, Sakmann and Neher developed a patch clamp technique that allowed them to measure the electrical currents across single ion channels (Neher and Sakmann, 1976). In 1986, Ashkin *et al.* invented optical tweezers that enabled several scientists to characterize many biomolecules at the single-molecule level by applying forces as small as several piconewtons (pN) and measuring nanometer-to-Angstrom-sized movements (Abbondanzieri *et al.*, 2005; Ashkin

et al., 1986, 1990; Block *et al.*, 1990; Bustamante *et al.*, 1994; Mehta *et al.*, 1999; Moffitt *et al.*, 2006; Vale *et al.*, 1985). In 1989, Moerner and Kador reported the first detection of single molecules in a solid at the cryo temperatures (Moerner and Kador, 1989). This was quickly followed in 1990 by Orrit and Bernard who dramatically improved the signal-to-noise ratio by using fluorescence (Orrit and Bernard, 1990). This was then followed by Soper *et al.*'s (1991) observation of single fluorophores at room temperature using far-field microscopy and Betzig *et al.*'s near-field optical microscopy (Betzig and Chichester, 1993; Betzig and Trautman, 1992). These discoveries and the invention (Axelrod, 1989) and use (Funatsu *et al.*, 1995; Vale *et al.*, 1996) of total internal reflection fluorescence microscopy (TIRF) led to imaging of single fluorophores and fluorescent proteins (FPs) using wide-field microscopy at room temperature. Since then, there has been a dramatic increase in the number of single-molecule experiments.

Modern super-resolution techniques such as single-molecule high-resolution imaging with photobleaching (SHRIMP) or single-molecule high-resolution colocalization (SHREC) rely on sequentially and accurately localizing single molecules (Balci *et al.*, 2005; Gordon *et al.*, 2004). SHRIMP achieves 10 nm resolution and uses two (or more) identical fluorophores (or FPs). One of the identical dyes is turned off by a permanent photobleaching, which occurs stochastically upon excitation. SHREC (Churchman *et al.*, 2005; Toprak and Selvin, 2007) and similar techniques (Michalet *et al.*, 2001) reach 8–10 nm resolution using two photostable organic fluorophores, or quantum dots (Lagerholm *et al.*, 2006; Lidke *et al.*, 2005), that have spectrally distinct wavelengths. Photoactivated localization microscopy (PALM) (Betzig *et al.*, 2006; Shroff *et al.*, 2007) and fluorescence photoactivated localization microscopy (FPALM) (Hess *et al.*, 2006), achieve about 25 nm resolution using photoactivatable fluorescent proteins (FAPs). FAPs are variants of FPs that can be turned on and off by a UV laser pulse, and then made to emit with a second longer-wavelength laser pulse. Stochastic optical reconstruction microscopy (STORM) is another super-resolution technique which essentially uses the same algorithm as (F)PALM. Although STORM formally includes FAPs, it mostly uses a wide variety of photoswitchable organic probes (Bates *et al.*, 2007; Huang *et al.*, 2008a). It also achieves about 25 nm resolution.

Finally, there are two methods for getting super-resolution that do not need single fluorophores. The first one is structured-illumination microscopy (SIM) (Gustafsson, 2005, 2008; Kner *et al.*, 2009). SIM can currently achieve twofold better ($\sim$120 nm) optical resolution than classical optical microscopy, although using nonlinear techniques, the resolution is formally unbounded. The second method is called stimulated emission depletion microscopy (STED; Hell, 2007; Hell and Wichmann, 1994; Klar *et al.*, 2000; Willig *et al.*, 2006). STED works by transiently turning off all fluorophores in the focal region, except those located at the zero of a

second, overlapping beam (the STED beam). It has achieved 16 nm resolution with organic fluorophores (Westphal and Hell, 2005) and 65 nm resolution at video rates (Westphal *et al.*, 2008). STED's ability to acquire data rapidly is one of the unique aspects of the technique, compared to the single-molecule methods.

Finally, improved optics and microscopy is only one part of the solution for achieving high-resolution images. In the case of fluorescence, there is the nontrivial problem of specifically labeling biomolecules, particularly in the cell. Fortunately, there are FPs, that is, green fluorescent protein (GFP) and its many different colored derivatives (Giepmans *et al.*, 2006; Shaner *et al.*, 2008). These are genetically encodable probes that enable perfect alignment with the biological molecule of interest. Of course, FPs have their own problems. They are not compatible with staining of tissue samples that are not already genetically encodable. There can also be problems of functionality because of the large size of FPs ($\sim$5 nm and larger for oligomers; Ormo *et al.*, 1996). More significantly, FPs are *not* sufficiently photostable and bright enough to see a single one (Shaner *et al.*, 2008). This is especially true if one wants to look for an extended period of time, that is, more than a few seconds. There are examples of single GFPs detected, particularly *in vitro* (Pierce *et al.*, 1997), and for six GFPs *in vivo* (Cai *et al.*, 2007), but photostability of FPs remains a major problem (Shaner *et al.*, 2008). Chemically synthesized organic fluorophores also have major problems, particularly for getting past the cell membrane and staining their targets specifically. The fluorophores are generally negatively charged to prevent them from aggregating, but this makes it very difficult to penetrate into the cell. Fluorescein derivatives, including fluorescein acetates/esters (Rotman and Papermaster, 1966) and FLASH (for fluorescein-based arsenical hairpin binder) and ReASH (for resorufin-based arsenical hairpin binder) (Griffin *et al.*, 1998), get through the membrane, but are not sufficiently photostable for single-molecule detection (Park *et al.*, 2004). Other dyes, such as tetramethylrhodamine, pass through the membrane but label nonspecifically. Finally quantum dots, which are very promising colloidal fluorescent particles, are very big ($>$3–20 nm) and therefore neither easily get into cells nor label organelles specifically (Michalet *et al.*, 2005).

2. Getting Super-Accuracy

Super-accuracy was first shown in a biological setting in 1996 when Schmidt *et al.* achieved 30 nm accuracy in single-molecule diffusion (Schmidt *et al.*, 1996). The *accuracy* with which you can determine the position of the particle is limited by the number of photons emitted (or absorbed), and a few other parameters. Figure 1.1 shows a (fluorescent) image of a single dye. The accuracy is determined by how well you can

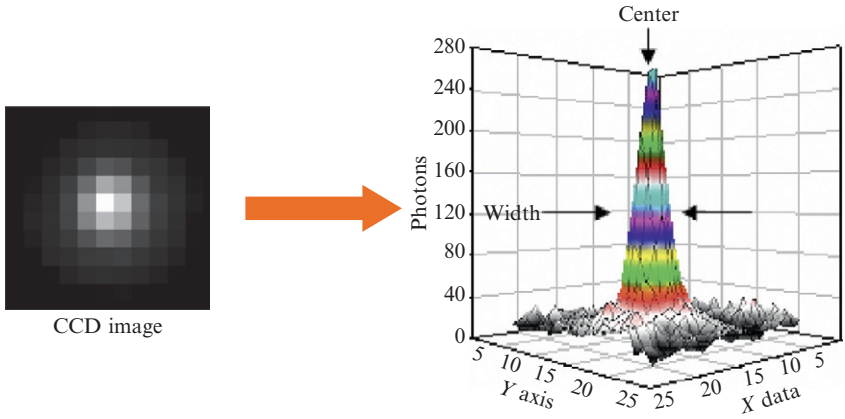

Figure 1.1 CCD image (left) of a fluorescent dye and corresponding emission pattern (right). The width (w) is ~250 nm, but the center can be located to within $w/\sqrt{N}$, where $N = 10^4$, is the total number of photons, making the center's uncertainty ±1.3 nm.

locate the center of the fluorescence distribution. Thompson *et al.* showed experimentally that they could localize a fluorescent bead with up to ~2 nm accuracy and derived a relationship for the accuracy (see Thompson *et al.*, 2002, Box 1). The accuracy is approximately equal to the width, or the diffraction limit of light, divided by the square root of the number of photons. The diffraction limit is typically $\lambda/2\text{NA}$ where λ is the wavelength of the emitted light and NA is the numerical aperture of the collecting lens. For visible light (λ~500 nm), NA = 1.4, and 14,000 photons collected in Fig. 1.1, one can locate the centroid of the distribution with ~1.3 nm accuracy. Obviously, this is much better than the diffraction limit of light.

There are a few other parameters that come into determining the accuracy. One is the size of the detection pixel with which the fluorescence is imaged. Obviously, if the pixel is too large, you cannot resolve the point spread function (PSF). If the pixel is too small, the signal-to-noise ratio diminishes and the PSF may become anisotropic (Enderlein *et al.*, 2006). In most cases, using ~85–120 nm (or a 150–250× magnification onto the typically 16–24 μm CCD (charge coupled devices) pixels) works well. The other issue is the background noise, either stemming from the detector, or from the sample in the form of autofluorescence. The former can be essentially eliminated with the advent of super-quiet, back-thinned, electron multiplying charge coupled devices (EMCCDs). Autofluorescence can be greatly minimized if your sample can be excited by a thin strip of light at the water–glass interface (Fig. 1.2). This is common, for example, in *in vitro* measurements where the sample is stuck down to the glass coverslip or slide, or *in vivo* measurements, where one is interested in looking at the cell

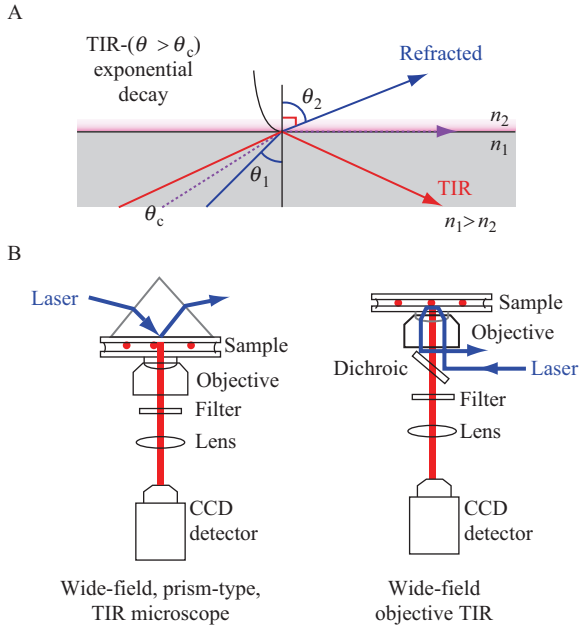

Figure 1.2 Schematics of total internal reflection. (A) In TIR, an excitation light enters a sample at a large angle such that it totally reflects at an glass (n_1)–water (n_2) interface. However, a small amount of energy enters the water, which exponentially dies away with about a 60 nm decay length. Consequently, fluorophores at the interface will be excited, but those beyond ~100 nm will not be excited. (B) There are two ways of exciting TIR. One is a prism type, and the other is an objective type. A prism type was initially the most popular, and still has certain advantage, but with objective lenses that are quieter, this has become the most popular and sensitive. Adapted from Selvin and Ha (2007).

membrane. The thin strip of light is created by exciting the sample with TIRF (Fig. 1.2).

In TIRF, the excitation light comes in at a large angle such that the light is totally internal reflected at the interface between the glass coverslip (or slide) and the water immersing the sample. Despite the complete reflection, there is a small amount of energy that reaches the sample. This energy dies away with a decay length ($1/e$) of ~60 nm, depending on the refractive indices of the two adjacent media. Hence, it excites your sample, but not the fluorophores above it. Of course, this is only good when the fluorescence is near the surface. A detailed description of building a custom-made TIRF setup for single fluorophore imaging can be found in the third chapter of the *Single Molecule Techniques* book edited by Selvin and Ha (2007).

Finally, there is a problem of how long the fluorescence lasts. We have found that adding the enzymes protocatechuic acid (PCA)/protocatechuate-3,4-dioxygenase (PCD) makes the fluorophores very stable, lasting from 30 s to several minutes (Aitken *et al.*, 2008). We initially used glucose oxidase and catalase, but found that the enzyme underwent some formulation changes (in the United States) and was no longer available in its original formulation (Yildiz *et al.*, 2003). (The catalase was made by Roche, from horses. In the United States, they switched to a molecular biology formulation, which we found did not work as well.)

3. Calculating Super-Accuracy

The fundamental goal is to determine the center, or mean value of the distribution, $\mu = (x_0, y_0)$, and its uncertainty, the standard error of the mean (σ_μ). σ_μ tells you how well you can localize the fluorophore. The relation between σ_μ and the number of collected photons (N), the pixel size of the imaging detector (a), the standard deviation of the background (b, which includes background fluorescence and detector noise), and the width of the distribution (standard deviation, s_i, in direction i) was derived by Thompson *et al.* (2002) in two dimensions:

$$\sigma_{\mu_i} = \sqrt{\left(\frac{s_i^2}{N} + \frac{a^2/12}{N} + \frac{8\pi s_i^4 b^2}{a^2 N^2}\right)} \tag{1.1}$$

where the index i refers to the x or y direction. The first term (s_i^2/N) is the photon noise, the second term is the effect of finite pixel size of the detector, and the last term is the effect of background.

Control experiments were done to demonstrate the ability to localize a translationally immobile dye. Figure 1.1 shows the PSF of an individual Cy3 dye attached to a coverslip via a DNA–biotin–streptavidin linkage, immersed in an aqueous buffer, and obtained with objective-type TIRF with an integration time of 0.5 s (Woehlke and Schliwa, 2000). For the highlighted PSF, $N = 14{,}200$ photons, $a = 86$ nm, $b = 11$, $s_y = 122$ nm, $s_x = 125$ nm (the full-width-half-max of the distribution, $\text{FWHM}_i = .354$ $s_i \approx 287$ nm). Based on Eq. (1.1), the expected σ_μ is 1.24 nm in each direction. Photon noise only (first term, Eq. (1.1)) leads to $\sigma_\mu = 1.02$ nm, pixelation (second term, Eq. (1.1)) increases σ_μ to 1.04 nm, and background noise (third term, Eq. (1.1)) increases σ_μ to 1.24 nm, showing that photon noise is the dominant contributor to σ_μ. A 2-D Gaussian yields an excellent fit ($r^2 = 0.994$; $\chi_r^2 = 1.48$; Woehlke and Schliwa, 2000, Fig. S2), with $\sigma_\mu = 1.3$ nm, in excellent agreement with the expected value. We note that fitting Fig. 1.1 with a 2-D Airy disk, which is formally the proper

function to use, rather than a 2-D Gaussian fit, does not lead to a significantly improved fit (Cheezum *et al.*, 2001). We now turn to various examples of FIONA, namely *in vitro*, *in vivo*, in living organism, and with nonfluorescent tags.

3.1. Kinesin walks hand-over-hand

Kinesin is a dimeric motor protein that walks processively along microtubules for several microns (Block *et al.*, 1990; Vale *et al.*, 1985; Yildiz *et al.*, 2004a). Kinesin is in charge of moving organelles and lipid vesicles toward the cellular membrane and has a step size of 8.3 nm (Svoboda *et al.*, 1993). This step size was measured using optical tweezers by attaching a micron-sized bead to the cargo-binding domain. Until 2004, there was an uncertainty about the walking mechanism of kinesin. One of the proposed models, known as the inchworm model, suggested that one of the two heads of kinesin was taking an 8.3 nm step and the other head followed this by another concerted 8.3 nm movement (Hua *et al.*, 2002; Yildiz *et al.*, 2004a). The other proposed model was a hand-over-hand model where each head was taking 16.6 nm steps and becoming the leading and trailing heads alternatingly. In 2004, two elegant back-to-back publications clearly showed that kinesin walks hand-over-hand. The first one was done using optical tweezers with a kinesin mutant that had a truncated stalk (Asbury *et al.*, 2003). In this work, Asbury *et al.* observed alternating fast and slow steps that suggested that both of the kinesin heads were equally responsible for generating steps via ATP hydrolysis. The second paper, published by Yildiz *et al.* (2004a), used FIONA for directly observing head movements. In this work, only one of the heads was labeled with a Cy3 dye. The expected head movements for the hand-over-hand mechanism were alternating $\sim$16.6 and $\sim$0 nm head movements. Indeed, this was the actual step size shown. Note that, in particular, the 0 nm step size could be inferred from this experiment. By plotting a histogram of the time between steps, one gets a function that looks like: $y(t) = k_1 k_2 (t e^{-k_1 t} + t e^{-k_2 t})/(k_1 - k_2)$, with each step occurring with a rate constant of k_i. With the two rates equal, this reduces to $y(t) = tk^2 \, e^{-kt}$. This result is clearly different from the exponential decay function expected if the underlying process is a single step and is Poissonian. The data agree very well with this model (Fig. 1.3D). Now we know that myosin V (Yildiz *et al.*, 2003), myosin VI (Yildiz *et al.*, 2004b), kinesin, and cytoplasmic dynein (Reck-Peterson *et al.*, 2006) all use the hand-over-hand mechanism. This is in contrast to an inchworm mechanism for certain nuclear (DNA) motors (Myong *et al.*, 2007).

The time resolution of early FIONA experiments was limited to 0.3–0.5 s since Cy3 or bifunctional rhodamine dyes were used, and CCD cameras were slower at that time. Now, we can accurately track single organic fluorophores using 20 ms exposure times (unpublished results), at

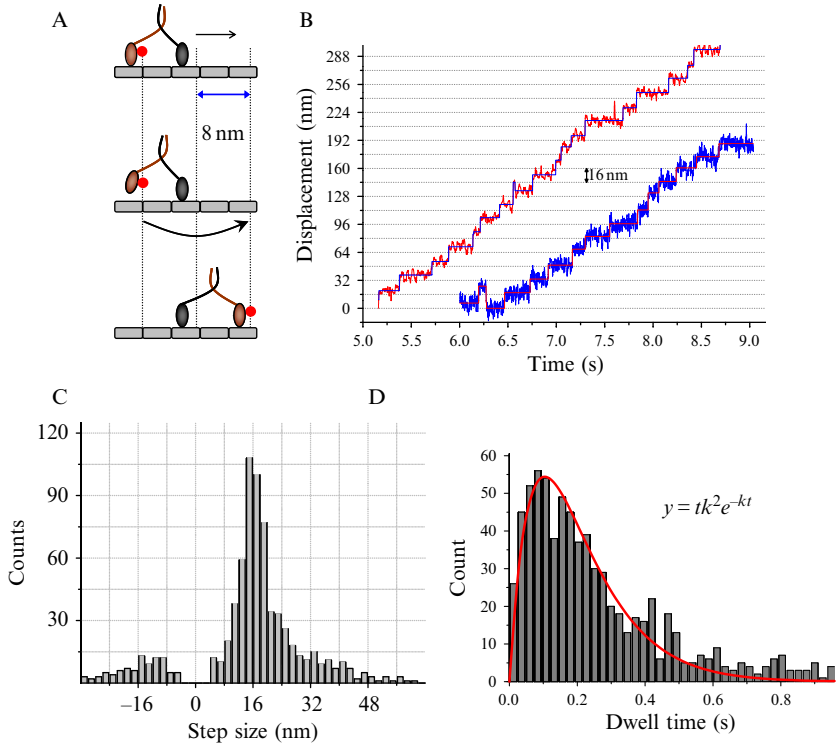

Figure 1.3 Stepping dynamics of kinesin molecules. (A) A kinesin molecule labeled with a quantum dot (red filled circle) on one of the microtubule-binding heads (brown). (B) Two sample traces of kinesin motility. Abrupt 16 nm steps were observed. (C) The step size distribution of quantum dot labeled kinesin molecules. (D) The hidden 0 nm step size can be detected because it leads to an initial linear rise. Adapted from Toprak *et al.* (2009).

the cost of less total time until photobleaching. A time resolution down to 1 ms when tracking quantum dots is possible. This advance is important for showing how kinesin acts *in vitro* at higher ATP concentrations (Toprak *et al.*, 2009) and for *in vivo* measurements (Kural *et al.*, 2005; also see later). As an *in vitro* example, we labeled kinesin's microtubule-binding head with a streptavidin-coated quantum dot (QS655, Molecular Probes; Fig. 1.3B). We imaged kinesin molecules using 2 or 4 ms exposure times at 5 μM ATP. This ATP concentration is 16-fold higher and the time resolution 125–250-fold faster than for our original experiments using Cy3 dyes. We clearly observed abrupt $\sim$16 nm steps (Fig. 1.3B) (Toprak *et al.*, 2009). The average step size was 16.3 $\pm$ 4.4 nm (Fig. 1.3C).

Also, with quantum dots, because they are so bright, enough photons can be collected to detect small step sizes. The center-of-mass steps of

kinesin, for example, has been measured with FIONA to be 8.4 ± 0.7 nm (Yardimci *et al.*, 2008), in good agreement with the optical trap value of 8.3 nm (Svoboda *et al.*, 1993). We note that the smallest step size that can be measured is often not limited by the amount of photons, but rather by the noise sources such as drift and vibrations.

3.2. Kinesin and dynein *in vivo*

It is of course desirable to look at molecular motors inside a cell (Kural *et al.*, 2005). For this goal, we had two problems: how to label them with a photostable dye, and how to reach high enough of a time resolution given that the [ATP] is about 2 mM within cells, greatly accelerating the motor. As mentioned before, it is very difficult to use single fluorophores inside the cell. Hence, we tracked movements of fluorescently tagged organelles, such as peroxisomes, for studying the dynamics of motor proteins. Because there were hundreds of GFPs per peroxisome, but they all moved together, the criteria held for determining the position of a single molecule with high precision. Furthermore, the GFPs were surprisingly photostable. Fortunately, the time resolution we needed was about 1 ms, which was just accessible with our fastest (Andor) EMCCD camera.

Figure 1.4 is the result. We found that the peroxisomes moved in 8.3 nm steps, which was the value for kinesin and dynein step sizes *in vitro*. Even more interestingly, we saw that peroxisomes undergo a saltatory up-and-back motion, as is common among cargos. Presumably kinesin-1 is responsible for the forward motion, toward the positive-end of the microtubule, and dynein is responsible for the backwards motion, towards the negative-end. (Some more recent results suggest that dynein may be able to undergo forward and backward motion even in the absence of kinesin, possibly due to the presence of microtubule associated proteins (Dixit *et al.*, 2008) or dynactin (Vendra *et al.*, 2007).) How the transitions between the forward and backward motion occur remains unclear since they were faster than our time resolution.

3.3. FIONA without fluorescence

If sufficient contrast can be achieved in bright-field illumination, there is no reason to use fluorescence to accurately determine the centroid position of tiny organelles or vesicles. For tracking *Xenopus* melanosomes, which consist of dark melanin granules, bright-field illumination is sufficient. One advantage is that a simple microscope setup can be used, although we did use a rather sophisticated camera (a back-thinned EMCCD, Andor).

Figure 1.5 is one such example. An image is taken, inverted, and a 2-D Gaussian fit to the resulting PSF, which yields an accuracy of 2.4 nm with a 1 ms acquisition time. This result is verified by piezo-stepper experiments

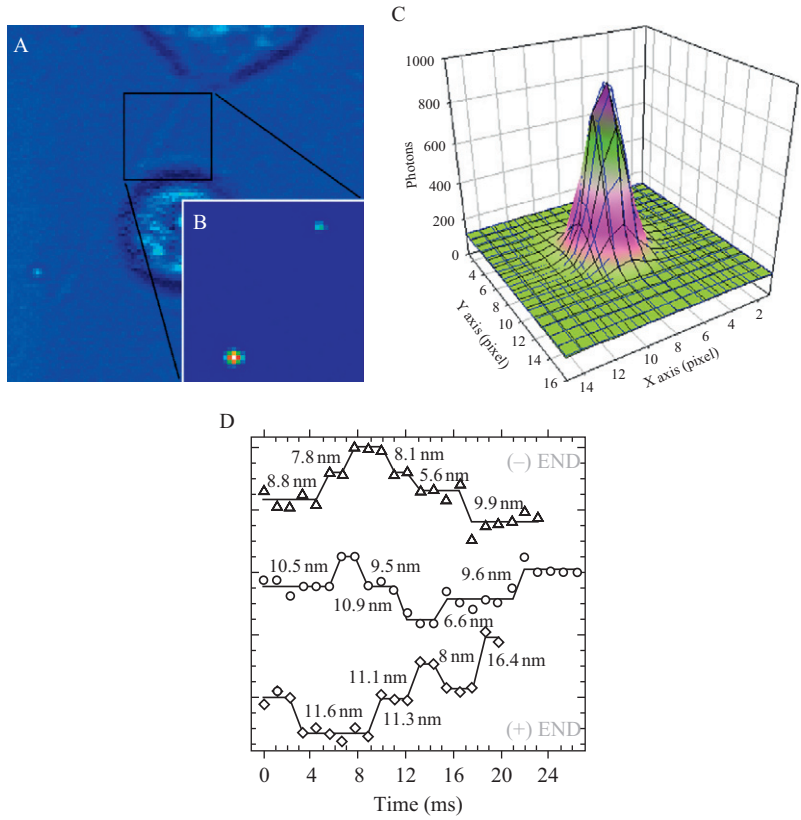

Figure 1.4 Kinesin and dynein steps can be detected *in vivo* using FIONA. (A) A bright-field image of a Drosophila S2 cell, with a process (long thick object) sticking out of it due to actin depolymerization. (B) Looking at the rectangular area via fluorescence microscopy, two GFP-peroxisomes are visible. The time resolution was 1.1 ms. (C) The PSF of the GFP-peroxisomes are plotted and the center was determine with an accuracy of be 1.5 nm. (D) The movement of a cargo being moved *in vivo* by either dynein, going away from the nucleus (the (−)-ve direction), or kinesin, going towards the nucleus (the (+)-ve direction), or switching between the two motors. It walks with 8 nm center-of-mass. Adapted from Kural *et al.* (2005).

performed on fixed melanophores where steps of 8 nm can be easily resolved by using this tracking scheme. We named this technique bright-field imaging with one nanometer accuracy (bFIONA) (Kural *et al.*, 2007). Since bFIONA tracking does not depend on fluorescence, high spatial resolution is not limited by photobleaching. Furthermore, the absence of toxic by-products of photobleaching, such as oxygen radicals, makes bFIONA an appropriate tool to track organelles as long as desired, without severely harming cells.

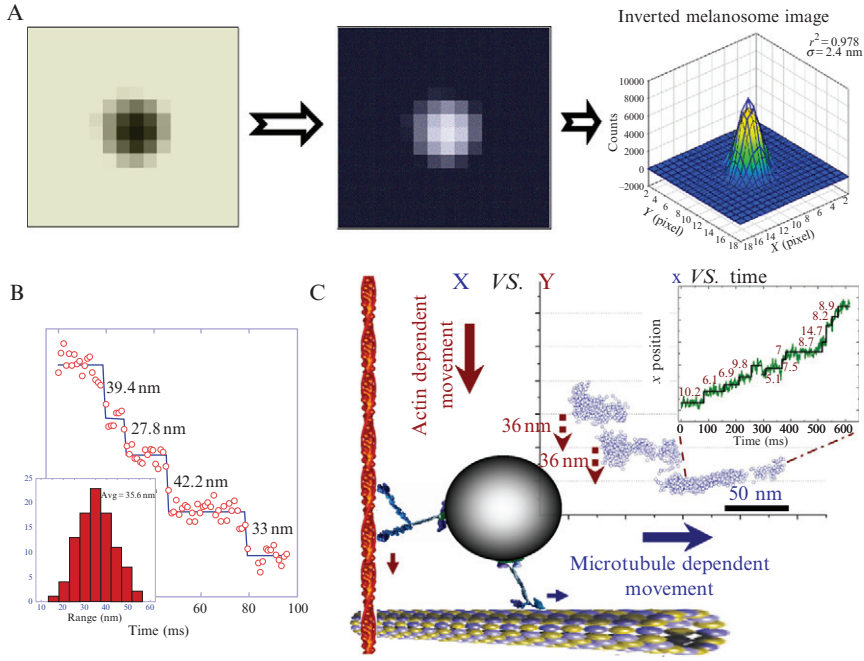

Figure 1.5 bFIONA. (A) The image of a dark melanosome is inverted and then plotted and fit to 2.4 nm accuracy. (B) Adding nocodozole depolymerizes the microtubules, leaving actin. The 36 nm center-of-mass steps are visible. (C) Both of the dyes can be tracked very accurately and one can see the transfer from actin to microtubules. Adapted from Kural *et al.* (2007).

By tracking melanosomes with bFIONA, we have shown that heterotrimeric kinesin-2 (KIF3) takes 8 nm steps (as in the case of conventional kinesin, KIF5). In cells where microtubules are depolymerized, we could resolve myosin V stepping as well. Our results also imply that intermediate filaments can hinder the movement of organelles in the cytoplasm since the uninterrupted run lengths of melanosome transport increased 1.5-fold in the absence of intermediate filaments.

3.4. FIONA in a live organism

Is it practical to use FIONA in a live organism, as opposed to *in vitro* or in cultured cells? To be able to address such a question one needs to make sure that the target organism can easily be labeled, which often means via genetic engineering, and be optically clear. The tiny nematode *Caenorhabditis elegans* was shown to be a perfect model organism for this purpose (Kural *et al.*, 2009). The subcellular compartments that belong to the neuronal system of

this worm can be tracked with sub-10 nm localization accuracy in a ~5 ms time resolution by FIONA.

Fluorescence imaging can be successfully performed on *C. elegans* because of its transparent body. Since the mechanosensory nerves are contiguous and aligned parallel to the cuticle, the fluorophores within these cells can be excited with TIR illumination if the worms can be immobilized adjacent to the coverslip. We have found that the ELKS proteins, which plays a regulatory role in synaptic development, can be imaged in a punctuate pattern in mechanosensory neurons when it is genetically labeled with GFP or photoconvertible DENDRA2 probes (Fig. 1.6A). 2-D Gaussian fits to the emission patterns of the fluorescent ELKS spots let us to localize the peak within 4.6 nm in 4 ms (Fig. 1.6B). The immobilization of the worms is performed by sandwiching them between a glass support and a coverslip. This is a very straightforward and effective way of performing stable measurements on simultaneous multiple worms without using anesthetic reagents that can alter the metabolism of the nematode. We have verified the vitality of the worms by making sure that their movement is restored after releasing the pressure between the glass layers.

Our results suggested that ELKS punctae are motionless in general, but are occasionally carried by molecular motors (Fig. 1.6C,D). In addition, we replaced the 15-protofilament microtubules with an 11-protofilament mutation. Even though this eliminates the touch sensitivity of the worms, it does not affect the organization and the punctuate pattern of ELKS. Other mutations that disrupt degenerin/epithelial Na^+ channel formation or interrupt their association with the epidermis (cuticle) also did not have an effect on the ELKS punctae distribution.

4. Reaching Super-Resolution

Optical resolution is the minimum distance necessary to distinguish two light emitting particles. If two objects are closer than the diffraction limit (λ/2NA), their PSFs overlap and you cannot tell that they are, in fact, two separate emitting objects (Fig. 1.7). If they are separated by a distance larger than the diffraction limit, their PSFs are well separated. To get improved resolution, one can try to decrease the width of individual PSFs, for example, by using a shorter wavelength of light; or one of the PSFs can be transiently or permanently photobleached (in SHRIMP, FPALM, STORM, or STED), or one can minimize the overlap of the PSFs, by, for example, making them spectrally distinct (in SHREC). We now go through several of these techniques, listed and summarized in section 1.

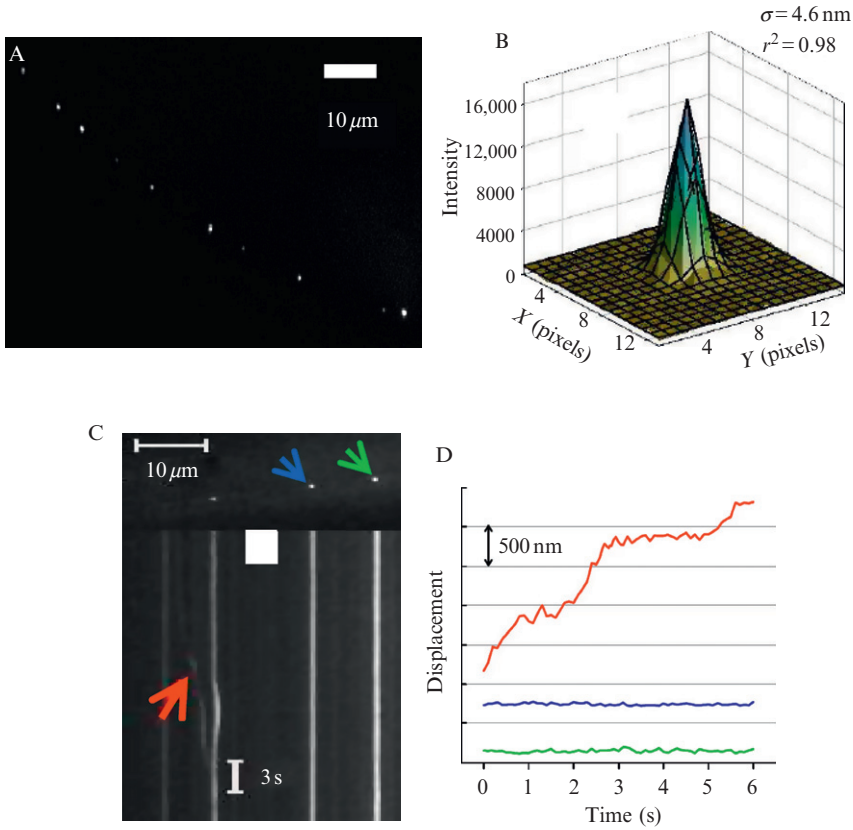

Figure 1.6 Fluorescently labeled protein complexes can be accurately localized within a live *C. elegans*. (A) DENDRA2::ELKS spots decorate the mechanosensory neurons along the *C. elegans* body. (B) The peak of the two dimensional Gaussian fit to the emission of a DENDRA::ELKS puncta can be localized within less than 5 nm in 4 ms. (C) A kymograph showing the moving and stationary GFP::ELKS spots in neurons. The displacement of spots pointed with red, blue and green arrows are shown in (D) with red, blue and green colors respectively. Adapted from Kural *et al.* (2009).

4.1. Single-molecule high-resolution imaging with photobleaching

If there are many fluorescent probes that are within a diffraction-limited spot, they appear to be a single bright spot. One solution is to sequentially switch off these fluorophores, and localizing them one by one. If the fluorophores are excited simultaneously, they will have a stochastic lifetime until photobleaching. Let us say there are two fluorophores, called A and B. If A photobleaches first, then B can subsequently be located with FIONA-type accuracy. Furthermore, A can then be localized in earlier images by

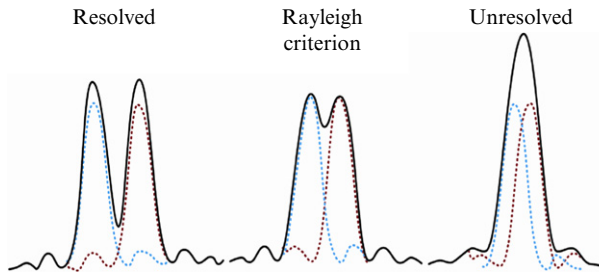

Figure 1.7 Two point particles at differing distances from each other create a well-resolved (left), a barely resolved (middle) or an unresolved image. If, however, the two PSF's can be resolved such that one particle at a time is imaged, then FIONA can be applied to each of them and their distances can theoretically be found to a few nanometers accuracy.

subtracting the photons of B from those of A + B, the former coming from the time following photobleaching. This technique was called single-molecule high-resolution imaging with photobleaching (SHRIMP). Figure 1.8 is an example of two dyes placed apart 329.7 ± 2.2 nm, where they can just be resolved by fitting a double-peaked Gaussian function to the two PSFs. They can also be resolved by SHRIMP, where we find 324.6 ± 1.6 nm. Smaller distances were successfully resolved by SHRIMP. However, smaller distances cannot be resolved by fitting multipeaked Gaussian functions. Gordon *et al.* (2004) labeled both ends of short DNA pieces (10, 17, and 51 nm) with two identical fluorophores in order to test the limits of SHRIMP. All of these distances were successfully resolved. Balci *et al.* (2005) later applied the same approach to measure the inter-head distance of myosin VI molecules labeled with GFPs on the actin-binding domains.

Qu *et al.* (2004) independently used the technique (which they called nanometer-localized multiple single-molecule (NALMS) fluorescence microscopy) to cover up to five separate fluorophores on DNA. We have recently applied this technique to study many—up to several hundred—fluorophores (P.R.S. Paul Simonson, unpublished data). One of the great advantages of SHRIMP is the convenience of using only one type of fluorophore for imaging. This feature increases fluorescent labeling efficiency and also makes imaging straightforward without having to correct any chromatic aberrations. A regular TIRF microscope can be used, although one may want a reasonably powerful laser to make the photobleaching time shorter.

4.2. Single-molecule high-resolution colocalization

SHREC was first introduced by Churchman *et al.* (2005) and later by Yildiz *et al.* (Toprak and Selvin, 2007). Using SHREC, one can measure distances larger than 10 nm that are out of the range of single-molecule fluorescence

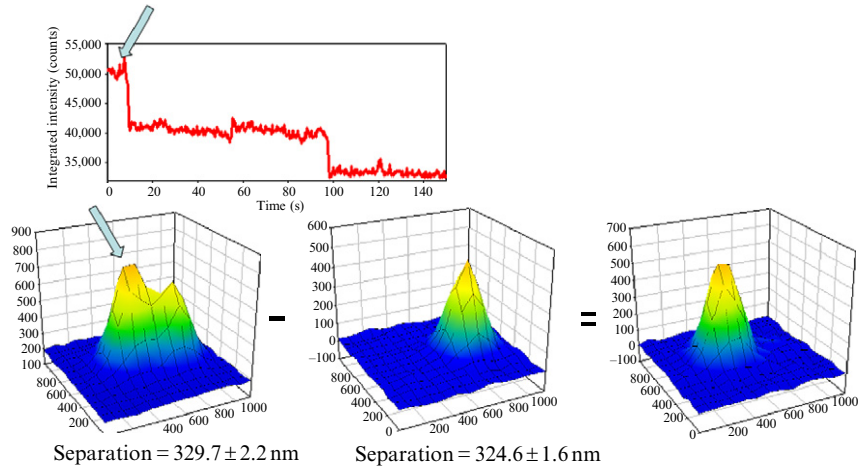

Figure 1.8 SHRIMP. Two fluorophores can be imaged (left). When one stochastically is photobleached, (arrow) the position of the other one can be fit to FIONA accuracy (middle). Subtracting this from the left-most image yields and fitting with FIONA, yields the position of the first dye. The agreement between SHRIMP technique, and normal fitting for (when the dyes are sufficiently far apart to be fit in the normal way), is excellent. The SHRIMP technique, however, has been shown to extend down to 10 nm. Adapted from Reference (Gordon *et al.*, 2004).

resonance energy transfer (FRET) and conventional light microscopy (Ha *et al.*, 1996). SHREC works by differentially labeling two sites of a biological molecule with two fluorophores that have spectrally different fluorescence emissions. Unlike FRET, both of the dyes are simultaneously excited with one or two lasers depending on the dyes. The resulting fluorescence emission is spectrally split using a homemade or commercial (e.g., a Dual-view, by Optical Insights) optical apparatus, and imaged with the same CCD (two separate CCD cameras can also be used if necessary). One common problem of the technique is the chromatic aberration in the imaging apparatus. That is, light emanating from a single spot consisting of two different wavelengths gets focused to different x, y, z spots. This interferes with the colocalization efficiency. After obtaining the images of both of the dyes, the images are localized on the CCD coordinates and these positions are mapped using a second (or higher) order polynomial. The standard way of assigning the mapping polynomial is imaging multicolor beads and colocalizing the spectrally split images so that the spectrally split emission of a fluorescent bead is mapped onto itself.

Churchman *et al.* used SHREC for measuring the length of short DNA segments that had Cy3 and Cy5 dyes on both ends. They successfully demonstrated that distances larger than 10 nm can be measured. They also monitored the movements of both of the two actin-binding heads of

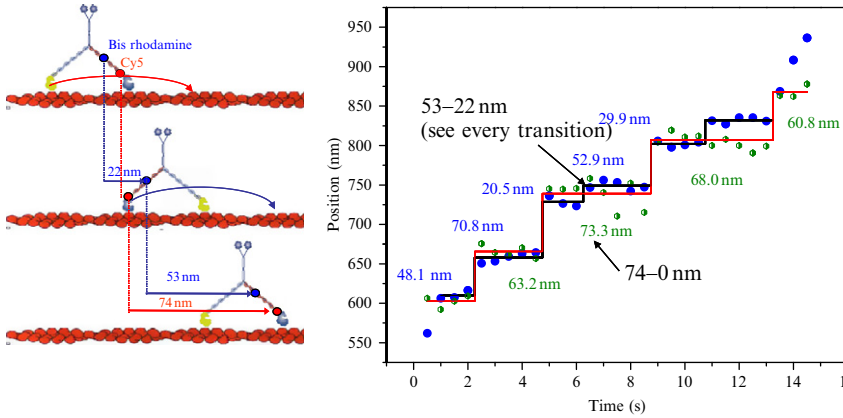

Figure 1.9 SHREC. Two fluorophores which emit at different wavelength can be imaged separately and the position of each dye fit with FIONA-like accuracy. The minimum distance between the two dyes, that is, the resolution, is approximately 10 nm. In this particular case, a myosin V, which moves with 37 nm center-of-mass, is labeled with a Bis-rhodamine (blue) and a Cy5 (red) (left). With the Cy5 labeled very close to the motor domain, a "hand-over-hand" motion causes the Cy5 to move 0-74-0-74 nm. The other dye, bis-rhodamine, labeled on the "leg," translocates by $(37-x)$ and $(37+x)$ nm, where x is the distance from the center-of-mass. Adapted from Toprak and Selvin (2007).

myosin V simultaneously. One of the heads was labeled with Cy3 and the other head was labeled with Cy5. Churchman *et al.* showed that each head was taking a 74 nm step after hydrolyzing an ATP molecule and the heads were alternating between trailing and leading positions. Similar experiments were later independently conducted by Yildiz *et al.* for exploring the stepping mechanism of myosin V further (Toprak and Selvin, 2007). As is shown in Fig. 1.9, two CaMs were differentially labeled with Cy3 and Cy5. The results were confirming the experiments of Churchman *et al.* except that a larger variety of events was observed since CaMs were labeled instead of the heads. Similar dynamics were also observed by Warshaw *et al.* (2005), where they used quantum dots instead of dyes. Similar approaches have been applied to photo-blinking quantum dots and fluorophores as well (Lidke *et al.*, 2005; Rosenberg *et al.*, 2005).

4.3. PALM and STORM

SHRIMP and SHREC are extremely effective when the number of fluorophores is limited. However, they are not sufficient to be able to resolve the structure of a complex molecule that is labeled with a high density of fluorophores. In order to overcome this difficulty, a number of groups

used a laser to activate a dye, and then another different-wavelength laser to excite the activated dye. Because only a small number of dyes were activated at any one time, very good resolution could be achieved. Two groups used PALM and FPALM based on a photoswitchable GFP (Patterson and Lippincott-Schwartz, 2002; often related to EosGFP; Wiedenmann *et al.*, 2004). They used intense irradiation with 413-nm wavelength, which increased fluorescence 100-fold upon excitation with 488-nm light. They showed that they could get ~25 nm resolution in fixed cells, although the initial observations took 24 h of microscopy time (Fig. 1.10; Betzig *et al.*, 2006; Hess *et al.*, 2006). One group has extended this to a second, differently colored FP and shortened the total time to 5–30 min (Shroff *et al.*, 2007). Unfortunately, this has not been achieved (yet) in living cells.

To get more colors in a photoswitchable way, STORM uses conjugates of two different organic fluorophores (Bates *et al.*, 2005, 2007; Huang *et al.*, 2008a, 2009). Formally, STORM includes all aspects of (F)PALM, including FAP, but often what is used are photoswitchable dyes. These had the surprising and favorable characteristic of being turned on and off several times (Bates *et al.*, 2005), as well as having many color combinations. The dye pair, called the "activator" and the "reporter" and both fluorescent probes, have to be in close proximity—a few nanometers—in order to facilitate photoswitching. (The photophysics is not really understood at this point.) For this purpose, the reporter and activator pairs can be conjugated to antibodies, double-stranded DNA molecules, or can be linked covalently. The reporter fluorophore is often a cyanine dye (generally Cy5, Cy5.5, or Cy7), and a proximal fluorophore with a shorter

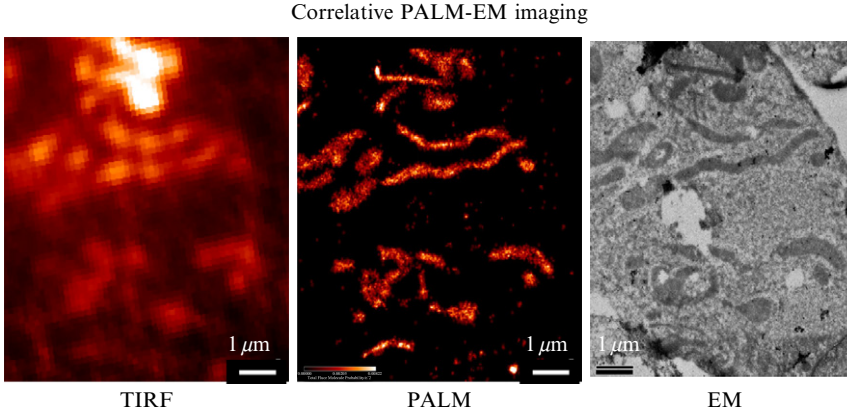

Figure 1.10 Images taken with TIRF, PALM, and by EM. The increased resolution of PALM is evident, and the structure correlates well with EM. Adapted from Betzig *et al.* (2006).

wavelength (e.g., Cy2 or Cy3) is used as the activator. Because a wide variety of activator–reporter pairs are available, it is possible to simultaneously use several different pairs, which give differing excitation or emission wavelengths. For example, the pairs Cy3–Cy5 and Cy3–Cy5.5 can both be used, where Cy3 requires a single wavelength to activate, but Cy5 and Cy5.5 emit at distinct wavelengths. Or Cy2–Cy5 and Cy3–Cy5 can be used where Cy2 and Cy3 require different excitation wavelengths but in both pairs the final signal (coming from Cy5 in both cases) is detected at the same wavelength. The latter has the advantage that chromatic aberrations do not have to be accounted for.

Molecules that are labeled with a high density of activator–reporter pairs can be imaged with sub-diffraction-limit resolution (up to 20 nm) with STORM (Fig. 1.11A). Only one dye pair is turned on in a diffraction-limited spot, and a FIONA-type image is taken. The process is then repeated many times, developing a high-resolution image. The Zhuang group managed to perform STORM on fixed cells where different intracellular molecules could be imaged in multiple colors (Bates *et al.*, 2007). They also could extend the high-resolution localization to the third (z) dimension with up to $\sim$50 nm axial resolution by making use of the ellipticity of individual PSFs introduced by cylindrical lenses inserted in the emission path (Fig. 1.11B; Huang *et al.*, 2008a).

A potentially important new derivative has been added to the STORM repertoire called direct STORM (dSTORM). It has the advantage of *not* using dimers of fluorophores. Rather it relies on a single fluorophore, sometimes in the presence of reducing agents, sometimes in the presence of air-saturated solution (van de Linde *et al.*, 2008, 2009). The molecules go into a metastable dark state and are hence turned off, while STORM is acquired. Approximately 20 nm resolution is achieved. Because only a single dye is used, there are no problems with chromatic aberrations, and it is very simple because only one excitation laser is used.

4.4. Stimulated emission depletion microscopy (STED)

Invented by Stefan Hell, STED is unlike other techniques in that it is not limited to single molecules. It also uses ''normal,'' albeit bright, fluorophores, rather than tandems of fluorophores. It also does not require any chromatic (or other) correction. In STED, as in conventional fluorescence techniques, a fluorophore is driven into its excited state and then proceeds to relax within a few picoseconds into the vibrationally lowest electronically excited state. At this point, it can make a transition to the ground state by either emission of a photon, that is, fluorescence, or nonradiative decay. So far, this is all the ''normal'' part of the fluorescence process. However, Hell applies a second beam that stimulates the excited state to spontaneously revert back down to a vibrationally upper state of the electronic ground state

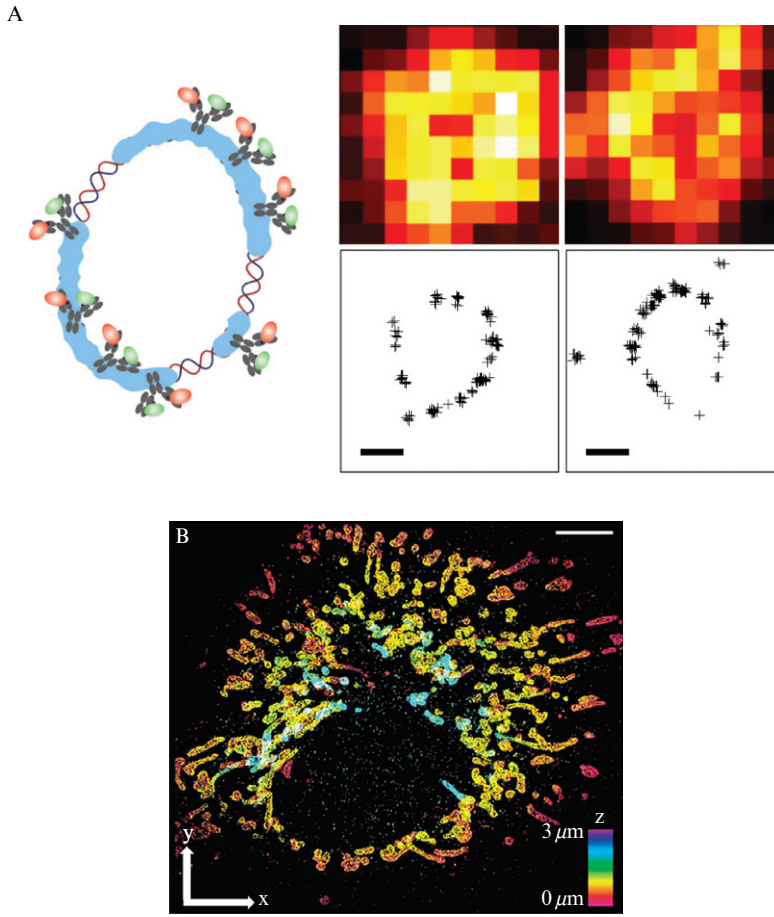

Figure 1.11 STORM can resolve structures smaller than the diffraction limit both in 2-D and 3-D. (A) RecA-coated circular DNA is imaged by immunofluorescence (top) and STORM images reconstructed as shown at the right (scale bars = 300 nm). (B) The mitochondrial network of a BS-C-1 cell is imaged with 3D STORM (scale bar = 1 mm). Adapted from Huang *et al.* (2008b).

(Fig. 1.12A). The probability for this event depends on the strength of the second beam. So, if a doughnut shape is made out of the beam, it will selectively depopulate those fluorophores (Fig. 1.12C), resulting in a sharper PSF and hence better spatial resolution. One of many impressive pictures of fixed cells is shown in Fig. 1.13.

Finally, Hell realized that the usual approximately twofold worse resolution in the z-axis ($\sim$500–700 nm) compared to the x–y axis ($\sim$200–300 nm) is due to the geometry, or symmetry, of the microscope objective. In the

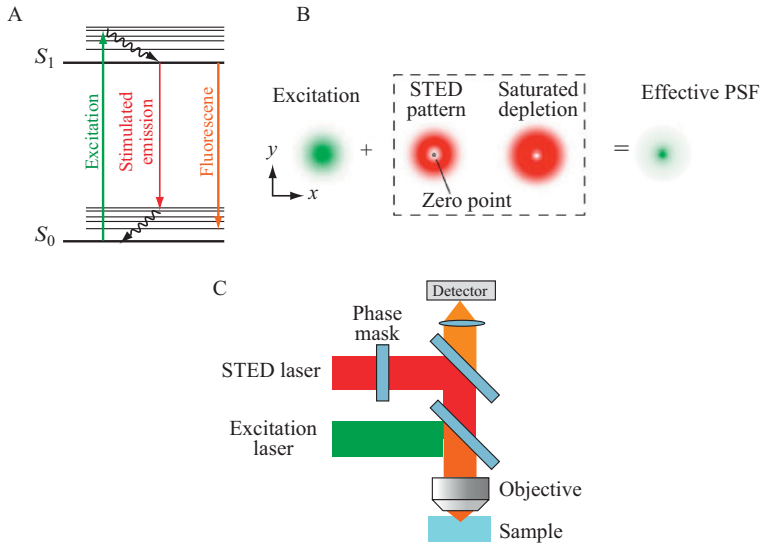

Figure 1.12 STED microscopy. STED consists of two laser beams: one which forms the normal fluorescence excitation beam (green); the other, called the STED laser, which causes relaxation of select fluorophores (red). These get forced to relax by stimulated emission. By putting in a phase mask in the STED laser, it can be made to form a doughnut-like shape. When combined with the excitation pulse, the result is a very narrow PSF. Adapted from Huang *et al.* (2009).

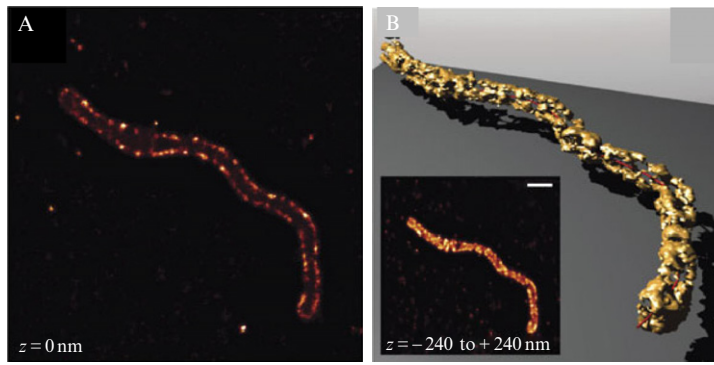

Figure 1.13 A variant of STED which forms a nearly spherical focal spots of 40–45 nm or *l*/16, in diameter. It can take a series of *z*-dimensions of a cell containing mitochondrion (A) and the image is then reconstructed (B). Reproduced with permission from Schmidt *et al.* (2008).

z-direction, only the light going towards the objective is collected, whereas in the x–y plane, all of the light is collected. The solution is to add another lens in the z-direction to collect more of the light. In addition, and most importantly, the sample is excited from both directions and the two beams interfere. The technique has been called 4Pi for scanning microscopy (Hell and Stelzer, 1992; Hell *et al.*, 2009), or I5M for wide-field illumination (Gustafsson *et al.*, 1999).

5. Future Directions

High accuracy and high-resolution microscopy has progressed tremendously in the past 10 or so years. A challenge that remains is to examine live cells, as the advances so far have been limited to *in vitro* samples and fixed cells. Looking at living cells, living specimens, and ultimately actual human tissues are the next steps. But here, the problem of autofluorescence and scattering is challenging. Perhaps nonlinear microscopy with its low scattering cross-sections is a favorable technique (Denk *et al.*, 1990; Larson *et al.*, 2003). New ways of specifically targeting fluorophores, especially smaller quantum dots (Michalet *et al.*, 2005; Smith and Nie, 2009), are badly needed. Perhaps then we can truly talk about seeing molecular changes in live samples in the optical microscope.

REFERENCES

Abbondanzieri, E. A., Greenleaf, W. J., Shaevitz, J. W., Landick, R., and Block, S. M. (2005). Direct observation of base-pair stepping by RNA polymerase. *Nature* **438**(7067), 460–465.

Aitken, C. E., Marshall, R. A., and Puglisi, J. D. (2008). An oxygen scavenging system for improvement of dye stability in single-molecule fluorescence experiments. *Biophys. J.* **94**(5), 1826–1835.

Asbury, C. L., Fehr, A. N., and Block, S. M. (2003). Kinesin moves by an asymmetric hand-over-hand mechanism. *Science* **302**(5653), 2130–2134.

Ashkin, A., Dziedzic, J. M., Bjorkholm, J. E., and Chu, S. (1986). Observation of a single-beam gradient force optical trap for dielectric particles. *Optics Lett.* **11,** 288–290.

Ashkin, A., Schutze, K., Dziedzic, J. M., Euteneuer, U., and Schliwa, M. (1990). Force generation of organelle transport measured in vivo by an infrared laser trap. *Nature* **348**(6299), 346–348.

Axelrod, D. (1989). Total internal reflection fluorescence microscopy. *Meth. Cell Biol.* **30,** 245–270.

Balci, H., Ha, T., Sweeney, H. L., and Selvin, P. R. (2005). Interhead distance measurements in myosin VI via SHRImP support a simplified hand-over-hand model. *Biophys. J.* **89**(1), 413–417.

Bates, M., Blosser, T. R., and Zhuang, X. (2005). Short-range spectroscopic ruler based on a single-molecule optical switch. *Phys. Rev. Lett.* **94**(10), 108101.

Bates, M., Huang, B., Dempsey, G. T., and Zhuang, X. (2007). Multicolor super-resolution imaging with photo-switchable fluorescent probes. *Science* **317**(5845), 1749–1753.

Betzig, E., and Chichester, R. J. (1993). Single molecules observed by near-field scanning optical microscopy. *Science* **262**(5138), 1422–1425.

Betzig, E., and Trautman, J. K. (1992). Near-field optics: Microscopy, spectroscopy, and surface modification beyond the diffraction limit. *Science* **257**(5067), 189–195.

Betzig, E., Patterson, G. H., Sougrat, R., Lindwasser, O. W., Olenych, S., Bonifacino, J. S., Davidson, M. W., Lippincott-Schwartz, J., and Hess, H. F. (2006). Imaging intracellular fluorescent proteins at nanometer resolution. *Science* **313**(5793), 1642–1645.

Block, S. M., Goldstein, L. S., and Schnapp, B. J. (1990). Bead movement by single kinesin molecules studied with optical tweezers. *Nature* **348**(6299), 348–352.

Bobroff, N. (1986). Position measurement with a resolution and noise-limited instrument. *Rev. Sci. Inst.* **57**(6), 1152–1157.

Bustamante, C., Marko, J. F., Siggia, E. D., and Smith, S. (1994). Entropic elasticity of lambda-phage DNA. *Science* **265**(5178), 1599–1600.

Cai, D., Verhey, K., and Meyhofer, E. (2007). Tracking single kinesin molecules in the cytoplasm of mammalian cells. *Biophys. J.* **92**(12), 4137–4144.

Cheezum, M. K., Walker, W. F., and Guilford, W. H. (2001). Quantitative comparison of algorithms for tracking single fluorescent particles. *Biophys. J.* **81**(4), 2378–2388.

Churchman, L. S., Okten, Z., Rock, R. S., Dawson, J. F., and Spudich, J. A. (2005). Single molecule high-resolution colocalization of Cy3 and Cy5 attached to macromolecules measures intramolecular distances through time. *Proc. Natl. Acad. Sci. USA* **102**(5), 1419–1423.

Denk, W., Strickler, J. H., and Webb, W. W. (1990). Two-photon laser scanning fluorescence microscopy. *Science* **248**(4951), 73–76.

Dixit, R., Ross, J. L., Goldman, Y. E., and Holzbaur, E. L. (2008). Differential regulation of dynein and kinesin motor proteins by tau. *Science* **319,** 1086–1089.

Enderlein, J., Toprak, E., and Selvin, P. R. (2006). Polarization effect on position accuracy of fluorophore localization. *Optic. Express* **14**(18), 8111–8120.

Funatsu, T., Harada, Y., Tokunaga, M., Saito, K., and Yanagida, T. (1995). Imaging of single fluorescent molecules and individual ATP turnovers by single myosin molecules in aqueous solution. *Nature* **374,** 555–559.

Gelles, J., Schnapp, B. J., and Sheetz, M. P. (1988). Tracking kinesin-driven movements with nanometre-scale precision. *Nature* **331**(6155), 450–453.

Ghosh, R. N., and Webb, W. W. (1994). Automated detection and tracking of individual and clustered cell surface low density lipoprotein receptor molecules. *Biophys. J.* **66**(5), 1301–1318.

Giepmans, B. N. G., Adams, S. R., Ellisman, M. H., and Tsien, R. Y. (2006). Review – The fluorescent toolbox for assessing protein location and function. *Science* **312**(5771), 217–224.

Gordon, M. P., Ha, T., and Selvin, P. R. (2004). Single-molecule high-resolution imaging with photobleaching. *Proc. Natl. Acad. Sci. USA* **101**(17), 6462–6465.

Griffin, B. A., Adams, S. R., and Tsien, R. Y. (1998). Specific covalent labeling of recombinant protein molecules inside live cells. *Science* **281,** 269–272.

Gustafsson, M. G. (2005). Nonlinear structured-illumination microscopy: Wide-field fluorescence imaging with theoretically unlimited resolution. *Proc. Natl. Acad. Sci. USA* **102**(37), 13081–13086.

Gustafsson, M. G., Agard, D. A., and Sedat, J. W. (1999). I5M: 3D widefield light microscopy with better than 100 nm axial resolution. *J. Microsc.* **195**(Pt 1), 10–16.

Gustafsson, M. G., Shao, L., Carlton, P. M., Wang, C. J., Golubovskaya, I. N., Cande, W. Z., Agard, D. A., and Sedat, J. W. (2008). Three-dimensional resolution doubling in wide-field fluorescence microscopy by structured illumination. *Biophys. J.* **94**(12), 4957–4970.

Ha, T., Enderle, T., Ogletree, D. F., Chemla, D. S., Selvin, P. R., and Weiss, S. (1996). Probing the interaction between two single molecules: Fluorescence resonance energy transfer between a single donor and a single acceptor. *Proc. Natl. Acad. Sci. USA* **93**(13), 6264–6268.

Hell, S. W. (2007). Far-field optical nanoscopy. *Science* **316**(5828), 1153–1158.

Hell, S., and Stelzer, E. H. K. (1992). Fundamental improvement of resolution with a 4Pi-confocal fluorescence microscope using two-photon excitation. *Optics Comm.* **93,** 277–282.

Hell, S. W., and Wichmann, J. (1994). Breaking the diffraction resolution limit by stimulated emission: Stimulated emission depletion microscopy. *Optic. Lett.* **19**(11), 780–782.

Hell, S. W., Schmidt, R., and Egner, A. (2009). Diffraction-unlimited three-dimensional optical nanoscopy with opposing lenses. *Nat. Photonics* **3,** 381–387.

Hess, S. T., Girirajan, T. P., and Mason, M. D. (2006). Ultra-high resolution imaging by fluorescence photoactivation localization microscopy. *Biophys. J.* **91**(11), 4258–4272.

Hua, W., Chung, J., and Gelles, J. (2002). Distinguishing inchworm and hand-over-hand processive kinesin movement by neck rotation measurements. *Science* **295**(5556), 844–848.

Huang, B., Wang, W., Bates, M., and Zhuang, X. (2008a). Three-dimensional super-resolution imaging by stochastic optical reconstruction microscopy. *Science* **319**(5864), 810–813.

Huang, B., Jones, S. A., Brandenburg, B., and Zhuang, X. (2008b). Whole-cell 3D STORM reveals interactions between cellular structures with nanometer-scale resolution. *Nat. Meth.* **5,** 1047–1052.

Huang, B., Bates, M., and Zhuang, X. (2009). Super-resolution fluorescence microscopy. *Annu. Rev. Biochem.* **78,** 993–1016.

Klar, T. A., Jakobs, S., Dyba, M., Egner, A., and Hell, S. W. (2000). Fluorescence microscopy with diffraction resolution limit broken by stimulated emission. *Proc. Natl. Acad. Sci. USA* **97**(15), 8206–8210.

Kner, P., Chhun, B. B., Griffis, E. R., Winoto, L., and Gustafsson, M. G. (2009). Super-resolution video microscopy of live cells by structured illumination. *Nat. Meth.* **6**(5), 339–342.

Kural, C., Kim, H., Syed, S., Goshima, G., Gelfand, V. I., and Selvin, P. R. (2005). Kinesin and dynein move a peroxisome in vivo: A tug-of-war or coordinated movement? *Science* **308,** 1469–1472.

Kural, C., Serpinskaya, A. S., Chou, Y. H., Goldman, R. D., Gelfand, V. I., and Selvin, P. R. (2007). Tracking melanosomes inside a cell to study molecular motors and their interaction. *Proc. Natl. Acad. Sci. USA* **104,** 5378–5382.

Kural, C., Nonet, M. L., and Selvin, P. R. (2009). FIONA on the living worm, *Caenorhabditis elegans*. *Biochemistry* **48**(22), 4663–4665.

Lagerholm, B. C., Averett, L., Weinreb, G. E., Jacobson, K., and Thompson, N. L. (2006). Analysis method for measuring submicroscopic distances with blinking quantum dots. *Biophys. J.* **91**(8), 3050–3060.

Larson, D. R., Zipfel, W. R., Williams, R. M., Clark, S. W., Bruchez, M. P., Wise, F. W., and Webb, W. W. (2003). Water-soluble quantum dots for multiphoton fluorescence imaging in vivo. *Science* **300**(5624), 1434–1436.

Lidke, K., Rieger, B., Jovin, T., and Heintzmann, R. (2005). Superresolution by localization of quantum dots using blinking statistics. *Optic. Express* **13**(18), 7052–7062.

Mehta, A. D., Rief, M., Spudich, J. A., Smith, D. A., and Simmons, R. M. (1999). Single-molecule biomechanics with optical methods. *Science* **283**(5408), 1689–1695.

Michalet, X., Lacoste, T. D., and Weiss, S. (2001). Ultrahigh-resolution colocalization of spectrally separable point-like fluorescent probes. *Methods* **25**(1), 87–102.

Michalet, X., Pinaud, F. F., Bentolila, L. A., Tsay, J. M., Doose, S., Li, J. J., Sundaresan, G., Wu, A. M., Gambhir, S. S., and Weiss, S. (2005). Quantum dots for live cells, in vivo imaging, and diagnostics. *Science* **307**(5709), 538–544.

Moerner, W. E., and Kador, L. (1989). Optical detection and spectroscopy of single molecules in a solid. *Phys. Rev. Lett.* **62,** 2535–2538.

Moffitt, J. R., Chemla, Y. R., Izhaky, D., and Bustamante, C. (2006). Differential detection of dual traps improves the spatial resolution of optical tweezers. *Proc. Natl. Acad. Sci. USA* **103**(24), 9006–9011.

Myong, S., Bruno, M. M., Pyle, A. M., and Ha, T. (2007). Spring-loaded mechanism of DNA unwinding by hepatitis C virus NS3 helicase. *Science* **317,** 513–516.

Neher, E., and Sakmann, B. (1976). Single-channel currents recorded from membrane of denervated frog muscle fibres. *Nature* **260**(5554), 799–802.

Ormo, M., Cubitt, A. B., Kallio, K., Gross, L. A., Tsien, R. Y., and Remington, S. J. (1996). Crystal structure of the *Aequorea victoria* green fluorescent protein. *Science* **273**(5280), 1392–1395.

Orrit, M., and Bernard, J. (1990). Single pentacene molecules detected by fluorescence excitation in a p-terphenyl crystal. *Phys. Rev. Lett.* **65**(21), 2716–2719.

Park, H., Hanson, G., Duff, S., and Selvin, P. (2004). Nanometer localization of single ReAsH molecules. *J. Microsc.* **216,** 199–205.

Patterson, G. H., and Lippincott-Schwartz, J. (2002). A photoactivatable GFP for selective photolabeling of proteins and cells. *Science* **297**(5588), 1873–1877.

Pierce, D. W., Hom-Booher, N., and Vale, R. D. (1997). Imaging individual green fluorescent proteins. *Nature* **388**(6640), 338.

Qu, X., Wu, D., Mets, L., and Scherer, N. F. (2004). Nanometer-localized multiple single-molecule fluorescence microscopy. *Proc. Natl. Acad. Sci. USA* **101**(31), 11298–11303.

Reck-Peterson, S. L., Yildiz, A., Carter, A. P., Gennerich, A., Zhang, N., and Vale, R. D. (2006). Single-molecule analysis of dynein processivity and stepping behavior. *Cell* **126**(2), 335–348.

Rosenberg, S. A., Quinlan, M. E., Forkey, J. N., and Goldman, Y. E. (2005). Rotational motions of macro-molecules by single-molecule fluorescence microscopy. *Accounts Chem. Res.* **38**(7), 583–593.

Rotman, B., and Papermaster, B. W. (1966). Membrane properties of living mammalian cells as studied by enzymatic hydrolysis of fluorogenic esters. *Proc. Natl. Acad. Sci. USA* **55**(1), 134–141.

Schmidt, T., Schutz, G. J., Baumgartner, W., Gruber, H. J., and Schindler, H. (1996). Imaging of single molecule diffusion. *Proc. Natl. Acad. Sci. USA* **93**(7), 2926–2929.

Schmidt, R., Wurm, C. A., Jakobs, S., Engelhardt, J., Egner, A., and Hell, S. W. (2008). Spherical nanosized focal spot unravels the interior of cells. *Nat. Meth.* **5**(6), 539–544.

Selvin, P. R., and Ha, T. (2007). Single molecule techniques: A laboratory manual. Cold Spring Harbor, New York.

Shaner, N. C., Lin, M. Z., McKeown, M. R., Steinbach, P. A., Hazelwood, K. L., Davidson, M. W., and Tsien, R. Y. (2008). Improving the photostability of bright monomeric orange and red fluorescent proteins. *Nat. Meth.* **5**(6), 545–551.

Shroff, H., Galbraith, C. G., Galbraith, J. A., White, H., Gillette, J., Olenych, S., Davidson, M. W., and Betzig, E. (2007). Dual-color superresolution imaging of genetically expressed probes within individual adhesion complexes. *Proc. Natl. Acad. Sci. USA* **104**(51), 20308–20313.

Smith, A. M., and Nie, S. (2009). Next-generation quantum dots. *Nat. Biotechnol.* **27**(8), 732–733.

Soper, S. A., Shera, E. B., Martin, J. C., Jett, J. H., Hahn, H., Nutter, L., and Keller, R. A. (1991). Single-molecule detection of rhodamine-6G in ethanolic solutions using continuous wave laser excitation. *Anal. Chem.* **63**(5), 432–437.

Svoboda, K., Schmidt, C. F., Schnapp, B. J., and Block, S. M. (1993). Direct observation of kinesin stepping by optical trapping interferometry. *Nature* **365**(6448), 721–727.

Thompson, R. E., Larson, D. R., and Webb, W. W. (2002). Precise nanometer localization analysis for individual fluorescent probes. *Biophys. J.* **82**(5), 2775–2783.

Toprak, E., and Selvin, P. R. (2007). New fluorescent tools for watching nanometer-scale conformational changes of single molecules. *Annu. Rev. Biophys. Biomol. Struct.* **36,** 349–369.

Toprak, E., Yildiz, A., Hoffman, M. T., Rosenfeld, S. S., and Selvin, P. R. (2009). Why kinesin is so processive. *Proc. Natl. Acad. Sci. USA* **106,** 12717–12722.

Vale, R. D., Reese, T. S., and Sheetz, M. P. (1985). Identification of a novel force-generating protein, kinesin, involved in microtubule-based motility. *Cell* **42**(1), 39–50.

Vale, R. D., Funatsu, T., Pierce, D. W., Romberg, L., Harada, Y., and Yanagida, T. (1996). Direct observation of single kinesin molecules moving along microtubules. *Nature* **380** (6573), 451–453.

van de Linde, S., Kasper, R., Heilemann, M., and Sauer, M. (2008). Photoswitching microscopy with standard fluorophores. *Appl. Phys. B* **93,** 725–773.

van de Linde, S., Endesfelder, U., Mukherjee, A., Schuttpelz, M., Wiebusch, G., Wolter, S., Heilemann, M., and Sauer, M. (2009). Multicolor photoswitching microscopy for subdiffraction-resolution fluorescence imaging. *Photochem. Photobiol. Sci.* **8**(4), 465–469.

Vendra, G., Hamilton, R. S., and Davis, I. (2007). Dynactin suppresses the retrograde movement of apically localized mRNA in *Drosophila* blastoderm embryos. *RNA* **13,** 1860–1867.

Warshaw, D. M., Kennedy, G. G., Work, S. S., Krementsova, E. B., Beck, S., and Trybus, K. M. (2005). Differential labeling of myosin V heads with quantum dots allows direct visualization of hand-over-hand processivity. *Biophys. J.* **88**(5), L30–L32.

Westphal, V., and Hell, S. W. (2005). Nanoscale resolution in the focal plane of an optical microscope. *Phys. Rev. Lett.* **94,** 143903.

Westphal, V., Rizzoli, S. O., Lauterbach, M. A., Kamin, D., Jahn, R., and Hell, S. W. (2008). Video-rate far-field optical nanoscopy dissects synaptic vesicle movement. *Science* **320,** 246–249.

Wiedenmann, J., Ivanchenko, S., Oswald, F., Schmitt, F., Rocker, C., Salih, A., Spindler, K. D., and Nienhaus, G. U. (2004). EosFP, a fluorescent marker protein with UV-inducible green-to-red fluorescence conversion. *Proc. Natl. Acad. Sci. USA* **101**(45), 15905–15910.

Willig, K. I., Rizzoli, S. O., Westphal, V., Jahn, R., and Hell, S. W. (2006). STED microscopy reveals that synaptotagmin remains clustered after synaptic vesicle exocytosis. *Nature* **440**(7086), 935–939.

Woehlke, G., and Schliwa, M. (2000). Walking on two heads: The many talents of kinesin. *Nat. Rev. Mol. Cell. Biol.* **1**(1), 50–58.

Yardimci, H., van Duffelen, M., Mao, Y., Rosenfeld, S. S., and Selvin, P. R. (2008). The mitotic kinesin CENP-E is a processive transport motor. *Proc. Natl. Acad. Sci. USA* **105**(16), 6016–6021.

Yildiz, A., Forkey, J. N., McKinney, S. A., Ha, T., Goldman, Y. E., and Selvin, P. R. (2003). Myosin V walks hand-over-hand: Single fluorophore imaging with 1.5-nm localization. *Science* **300,** 2061–2065.

Yildiz, A., Tomishige, M., Vale, R. D., and Selvin, P. R. (2004a). Kinesin walks hand-over-hand. *Science* **303,** 676–678.

Yildiz, A., Park, H., Safer, D., Yang, Z., Chen, L. Q., Selvin, P. R., and Sweeney, H. L. (2004b). Myosin VI steps via a hand-over-hand mechanism with its lever arm undergoing fluctuations when attached to actin. *J. Biol. Chem.* **279**(36), 37223–37226.